Hindawi
Journal of Combustion
Volume 2018, Article ID 8924370, 11 pages
https://doi.org/10.1155/2018/8924370

Research Article

Prediction of Pollutant Emissions from Bluff-Body Stabilised Nonpremixed Flames

Nelu Munteanu and Shokri M. Amzaini

Western Norway University of Applied Sciences, N 5020 Bergen, Norway

Correspondence should be addressed to Nelu Munteanu; swed527@gmail.com

Received 10 February 2018; Accepted 6 June 2018; Published 2 September 2018

Academic Editor: Sergey M. Frolov

Construction of a stable flame is one of the critical design requirements in developing practical combustion systems. Flames stabilised by a bluff-body are extensively used in certain types of combustors. The design promotes mixing of cold reactants and hot products on the flame surface to improve the flame stability. In this study, bluff-body stabilised methane-hydrogen flames are computed using the steady laminar flamelet combustion method in conjunction with the Reynolds-averaged Navier-Stokes (RANS) approach. These flames are known as Sandia jet flames and have different jet mean velocities. The turbulence is modelled using the standard k-ϵ model and the chemical kinetics are modelled using the GRI-mechanism with 325 chemical reactions and 53 species. The computed mean reactive scalars of interest are compared with the experimental measurements at different axial locations in the flame. The computed values are in reasonably good agreement with the experimental data. Although some underpredictions are observed mainly for NO and CO at downstream locations in the flame, these results are consistent with earlier reported studies using more complex combustion models. The reason for these discrepancies is that the flamelet model is not adequate to capture the finite-rate chemistry effects and shear turbulence specifically, for species with a slow time scale such as nitrogen oxides.

1. Introduction

Combustion of fossil fuels has a severe impact on the environment and humankind. Environmental and health-related issues such as global warming, acid rain, and ocean acidification will continue to be at the forefront for years to come [1, 2]. The primary products generated from combustion are carbon dioxide (CO_2) and water (H_2O) among other primary pollutants such as nitrogen oxides (NO_x), sulphur oxides (SO_x), carbon monoxide (CO), unburned hydrocarbons (UHC), and particle matter (PM). For instance, an increase in CO_2 concentration would trap the heat in the atmosphere, and as a result, an increase in average global temperature is observed [3]. Nitrogen oxides and sulphur oxides react with water in the atmosphere and fall as acid rains causing a severe health and economic losses [2]. Subsequently, environmental regulations become stricter to minimise these pollutants. However, statics show that the contribution of renewable energy such as the wind, solar, and hydro is less than 8.4% according to the European Commission statistics in 2008 [4]. Therefore, replacing fossil fuels with another source of renewable energy especially for high energy density application such as the aviation sector is unlikely to be soon. Thus, engineers and scientists are required to develop cleaner combustion systems that meet the environmental legislation demands and at the same time maintain high efficiency.

Mixing the reactants is crucial in sustaining combustion. For instance, if the mixture is inhomogeneous, some regions will have a higher equivalence ratio creating pockets with elevated temperature, which lead to NOx formation [5]. Furthermore, the stability of lean premixed flames can reduce the efficiency and the lifetime of the combustion device [6]. Construction of a stable flame is one of the critical design requirements in developing practical combustion systems [7, 8]. Flames stabilised by a bluff-body are extensively used in certain types of combustors. The design promotes mixing of cold reactants and hot products on the flame surface and improves the flame stability.

The primary challenge in turbulent combustion modelling is to find a physically and chemically meaningful

closure for the mean reaction rate, $\widetilde{\dot{\omega}_\alpha}$, which appears in the species transport equation. This term is nonlinear and evaluating it from the mean temperature and species concentration is known to be inappropriate [10]. RANS-Flamelet-based methods are widely used in industry and research for both premixed [11–14] and nonpremixed combustion [11, 15, 16]. Despite its limitation, the method is capable of predicting the interaction between turbulence and chemical reaction. Hence, the aim of this work is to predict pollutants from nonpremixed flames stabilised by a bluff-body. These flames were investigated in previous experimental studies [17, 18].

The outline of this paper is as follows. In Section 2, the flamelet method for nonpremixed flames with its assumptions and limitations is discussed. In Section 3, the chosen test flames are presented. The computational details are discussed in Section 4. The outcome of this study is discussed in Section 5. Finally, the summary and conclusion of this study are discussed in the last section.

2. Flamelet Model Formulation

The fundamental principle of the flamelet-based methods is to presume the turbulent flame structure as a collection of laminar flamelets that are locally one-dimensional [11]. This assumption is satisfactory when the flame characteristic turbulence scales are much larger compared with the flame scales, and consequently, turbulence eddies do not penetrate and disturb the flame structure. The deviation from the flamelet regime and the relation between these scales is given by Damköhler number, which is defined as $Da = \tau_t/\tau_c$. τ_t and τ_c denote the turbulent and chemical time scale, respectively. These laminar flames are usually characterised using a passive scalar mixture fraction (z), which measures the ratio between fuel and oxidiser. The values of mixture fraction are set to be 1 in the fuel and 0 in the oxidiser.

In the steady laminar flamelet method, the mean scalars of interest are parametrised using the mixture fraction, z, and the scalar dissipation rate (χ) which is broadly defined as the rate at which turbulence-generated fluctuations in the mixture fraction are dissipated. Scalar dissipation can disturb the structure of the laminar flamelet by stretching the reaction zone. It is to be noted that, at low strain rate values, the structure of the laminar flamelet resembles the equilibrium state, and at high values, flame extinction takes place. The computational tool used in this study solves the scalar dissipation rate with an initial value that is specified to be 0.2 and continuously increases until the maximum scalar dissipation rate is reached, or the flame has extinguished. The scalar dissipation rate, χ, is defined as

$$\chi = 2D\left(\frac{\partial z}{\partial x_i}\right)^2, \tag{1}$$

where D is the diffusion coefficient. The scalar dissipation χ varies along the axis of the flamelet. The stretch effects and quenching at stoichiometry are accounted by χ_{st} [19]. For a counter-flow flame, the flamelet strain rate, a_s, is related to the scalar dissipation at the location where z is stoichiometric by

$$\chi_{st} = \frac{a_s\left(-2\left[erfc^{-1}\left(2z_{st}\right)\right]^2\right)}{\pi}, \tag{2}$$

where χ_{st} is the stoichiometric scalar dissipation rate at the stoichiometric mixture fraction, z_{st}. a_s is the strain rate, and $erfc^{-1}$ is the inverse complementary error function.

In the tabulated approach, a set of one-dimensional instantaneous species mass fraction $Y_\alpha(z, \chi_{st})$ (4) and the instantaneous temperature $T(z, \chi_{st})$ (7) with different values of χ_{st} are solved with detailed reaction mechanisms to account for nonequilibrium and finite-rate chemistry effects [11]. These scalars are tabulated as a function of mixture fraction and dissipation rate as follows:

$$\phi = \phi\left(Z, \chi\right). \tag{3}$$

The instantaneous transport equation of species concentration is expressed as

$$\rho\frac{\partial Y_\alpha}{\partial t} - \frac{1}{2}\rho\chi\frac{\partial^2 Y_\alpha}{\partial z^2} - \dot{\omega}_\alpha = 0. \tag{4}$$

The first term in (4) denotes the unsteady changes of species mass fraction, Y_α. The second term represents the diffusion of species, Y_α. The third term represents the instantaneous reaction rate and is given by

$$\dot{\omega}_k = k_{f_k}\prod_{\alpha=1}^{n}\left(\frac{\rho Y_\alpha}{W_\alpha}\right)^{\nu'_{\alpha k}} - k_{b_k}\prod_{\alpha=1}^{n}\left(\frac{\rho Y_\alpha}{W_\alpha}\right)^{\nu''_{\alpha k}}. \tag{5}$$

k_{f_k} and k_{b_k} represent the forward and backward reaction rate coefficients, respectively. W_α is the molecular weight of species α. $\nu'_{\alpha k}$ and $\nu''_{\alpha k}$ are the forward and backward stoichiometric coefficient, respectively. The forward and backward reaction rate coefficients are given by Arrhenius law: $k = AT^n\exp(-E_a/RT)$,where A, E_a denote the preexponential factor and the activation energy, respectively. The instantaneous chemical reaction of species, α, in mass basis can be expressed as

$$\dot{\omega}_\alpha = W_\alpha\sum_{k=1}^{n}\dot{\omega}_k\left(\nu''_{\alpha k} - \nu'_{\alpha k}\right). \tag{6}$$

The instantaneous transport equation of temperature is written as

$$\rho\frac{\partial T}{\partial t} - \frac{1}{2}\rho\chi\left(\frac{\partial^2 T}{\partial z^2} + \frac{1}{c_P}\frac{\partial c_P}{\partial z}\frac{\partial T}{\partial z}\right) + \frac{1}{c_p}\sum_{\alpha=1}^{n}h_\alpha\dot{\omega}_\alpha = 0. \tag{7}$$

The first term of (7) denotes the variation of the temperature, with time. The second term represents the diffusion of temperature, where T and c_P represent the temperature and the specific isobaric and heat capacity, respectively. The third term represents the contribution from the production of species α. h_α denote the specific enthalpy of species α.

The Favre-averaged mean scalars of interest are then obtained using a Joint Probability Density Function of z and χ_{st} as follows:

$$\overline{\rho}\widetilde{\phi} = \int_0^\infty\int_0^1 \rho\phi\left(z, \chi_{st}\right)\widetilde{P}\left(z, \chi_{st}\right)dz\,d\chi_{st}, \tag{8}$$

Table 1: Characteristics of the flame B4F3A.

Flame	Mixture	D_J/D_B [mm]	U_J/U_{CO} [m/s]	Re_J	T[K]	ϕ
B4F3A	CH_4/H_2(1:1)	3.6/50	118/40	15800	298	0.05

where $\widetilde{p}(z, \chi_{st})$ is the probability density function of z and χ_{st} and is given by $\widetilde{p}(z, \chi_{st}) = \widetilde{p}(z)\widetilde{p}(\chi_{st})$. $\widetilde{p}(z)$ is closed using a presumed shape with a Beta function as follows [20]:

$$\widetilde{p}(z) = Cz^{a-1}(1-z)^{b-1}, \tag{9}$$

where C denotes the inverse of the normalisation factor and is given by $C = 1/\beta(a, b)$. a and b denote the parameters of Beta function and are given by $a = \widetilde{z}(\nu - 1)$ and $b = (1 - \widetilde{z})(\nu - 1)$. ν is the variance parameter given by $\nu = \widetilde{z}(1 - \widetilde{z})/\widetilde{z''^2}$. The normalisation factor is given by $\beta(a, b) = \int_0^1 z^{a-1}(1 - z)^{b-1}dz$. $\widetilde{p}(\chi_{st})$ is given by a Dirac-delta as follows [20]:

$$\widetilde{p}(\chi_{st}) = \delta(\chi_{st} - \widetilde{\chi}_{st}). \tag{10}$$

The mean mixture fraction, $\widetilde{z}$, is obtained from the following transport equation:

$$\frac{\partial \overline{\rho}\widetilde{z}}{\partial t} + \frac{\partial}{\partial x_i}\left(\overline{\rho}\widetilde{u}_i\widetilde{z}\right) = \frac{\partial}{\partial x_i}\left(\overline{\rho D\frac{\partial z}{\partial x_i}} - \overline{\rho}\widetilde{u_i''z''}\right). \tag{11}$$

The turbulent scalar flux is closed using the classical gradient assumption and is given by $\overline{\rho}\widetilde{u_i''z''} = (-\mu_t/S_{ct})(\partial\widetilde{z}/\partial x_i)$. μ_t denotes the viscosity and S_{ct} denotes the turbulent Schmidt number. The turbulent viscosity is closed by $\mu_t = \overline{\rho}C_\mu(\widetilde{k^2}/\widetilde{\varepsilon})$.

The mean mixture fraction variance is obtained from the following transport equation:

$$\begin{aligned}\frac{\partial \overline{\rho}\widetilde{z''^2}}{\partial t} &+ \frac{\partial}{\partial x_i}\left(\overline{\rho}\widetilde{u}_i\widetilde{z''^2}\right)\\ &= \frac{\partial}{\partial x_i}\left(\overline{\rho D\frac{\partial z''^2}{\partial x_i}} - \overline{\rho u_i''z''^2}\right) - 2\overline{\rho u_i''z''}\frac{\partial \widetilde{z}}{\partial x_i}\\ &\quad - 2\overline{\rho D\frac{\partial z''}{\partial x_i}\frac{\partial z''}{\partial x_i}}.\end{aligned} \tag{12}$$

The terms on the L.H.S denote the time variation and convection of $\widetilde{z''^2}$. The terms into the brackets on the R.H.S account for the molecular diffusion and turbulent scalar transport. The second term represents the production of z'', where the unknown $\overline{\rho u_i''z''}$ is modelled using the gradient assumption. The third term on the R.H.S represents the dissipation rate and is given by

$$\overline{2\rho D\frac{\partial z''}{\partial x_i}\frac{\partial z''}{\partial x_i}} = \widetilde{\chi} = C_\chi\frac{\widetilde{z''^2}}{\tau_t} = C_\chi\frac{\widetilde{\varepsilon}}{\widetilde{k}}\widetilde{z''^2}, \tag{13}$$

$\widetilde{k}$ and $\widetilde{\varepsilon}$represent the mean kinetic energy and its dissipation rate, respectively. C_χ is a constant given by C_χ= 2 [21]. Two transport equations for the mean $\widetilde{k}, \widetilde{\varepsilon}$ are solved and written as

$$\begin{aligned}\frac{\partial}{\partial t}\left(\overline{\rho}\widetilde{k}\right) &+ \frac{\partial}{\partial x_i}\left(\overline{\rho}\widetilde{u}_i\widetilde{k}\right)\\ &= \frac{\partial}{\partial x_i}\left[\left(\mu + \frac{\mu_t}{\sigma_{\widetilde{k}}}\right)\frac{\partial \widetilde{k}}{\partial x_i}\right] + \overline{\rho}\tau_{ij}\frac{\partial \widetilde{u}_j}{\partial x_i} - \overline{\rho}\widetilde{\varepsilon},\end{aligned} \tag{14}$$

and

$$\begin{aligned}\frac{\partial}{\partial t}\left(\overline{\rho}\widetilde{\varepsilon}\right) + \frac{\partial}{\partial x_i}\left(\overline{\rho}\widetilde{u}_i\widetilde{\varepsilon}\right) &= \frac{\partial}{\partial x_i}\left[\left(\mu + \frac{\mu_t}{\sigma_{\widetilde{\varepsilon}}}\right)\frac{\partial \widetilde{\varepsilon}}{\partial x_i}\right]\\ &\quad + C_{\widetilde{\varepsilon}_1}\frac{\widetilde{\varepsilon}}{\widetilde{k}}\overline{\rho}\tau_{ij}\frac{\partial \widetilde{u}_j}{\partial x_i} - C_{\widetilde{\varepsilon}_2}\overline{\rho}\frac{\widetilde{\varepsilon}^2}{\widetilde{k}}.\end{aligned} \tag{15}$$

The standard model constants [22, 23] are $C_\mu = 0.09$, $\sigma_k = 1.0$, $\sigma_\varepsilon = 1.30$,$C_{\varepsilon_1} = 1.44$, and $C_{\varepsilon_2} = 1.92$.

3. Test Flames

The test flames chosen to test the flamelet method are the nonpremixed bluff-body flames described in [17, 18]. The burner consists of a centre jet with a diameter of 3.6 mm and a bluff-body with a diameter of 50 mm, showed in Figure 1. The burner is surrounded by a co-flow tunnel with the following dimensions D_{CO}=305x 305 mm. The main jet contains a (50/50% by volume) mixture of methane and hydrogen with an initial temperature of 293K. Three flames were considered in the experiment and are labelled as B3F3A, B3F3B, and B3F3C with different jet velocities of 118, 178, and 217 m/s, respectively. The Reynolds number Re_j, which is defined based on the main jet bulk velocity U_j and integral length scale D_j, is 15800, 23900, and 28700, respectively. The B4F3A flame, which has the lowest jet velocity, is considered to test flamelet method. The characteristics of the selected flame are summarised in Table 1. The major and minor species concentrations are measured using Raman/ Rayleigh/ LIF technique at different radial and axial locations in the flame [24]. To minimise the heat losses, the bluff-body is coated with a ceramic layer. The bluff-body creates a recirculation zone to substantially improve the flame stability over an extensively range of co-flow and jet conditions [8, 25]. These flames have been used to validate different combustion models such as conditional moment closure (CMC) [26], probability density function (PDF) [27], and flamelet [28].

4. Computational Details

The computational tool used in this study is the commercial software Star CCM+. The tool solves the steady Favre-averaged transport equations for $\widetilde{z}$ and $\widetilde{z''^2}$ in (11) and (12) along with their appropriate closures on the physical grid.

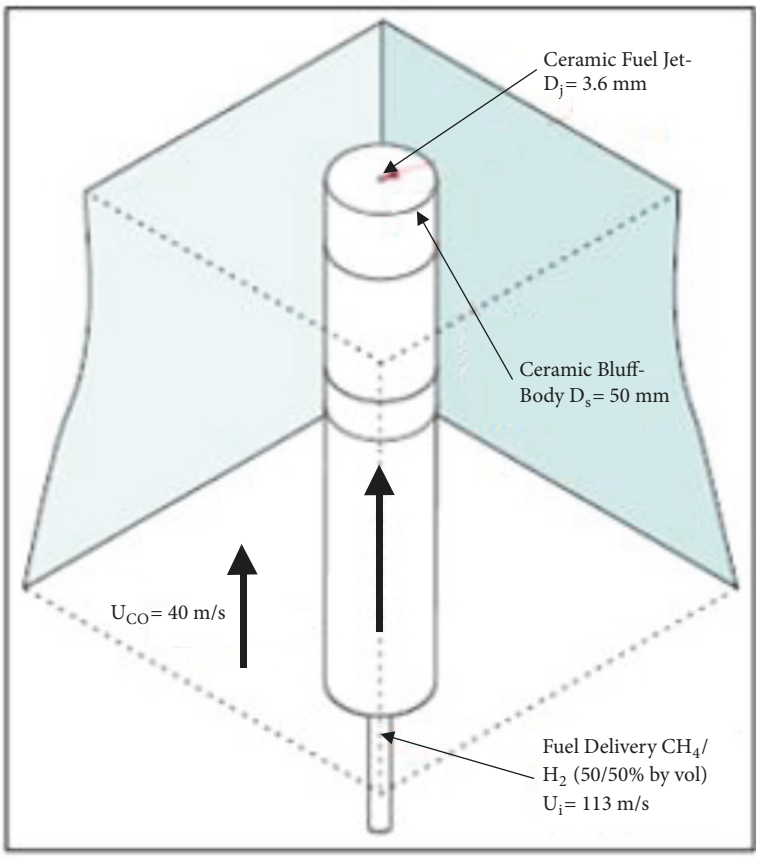

Figure 1: Schematic diagram of the flame B4F3A.

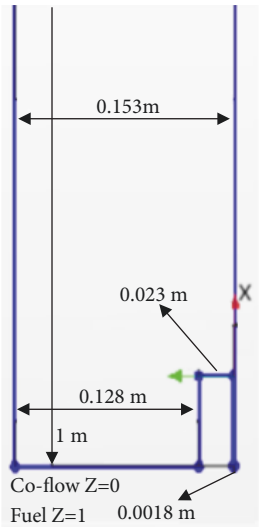

Figure 2: Computational domain dimension.

The turbulence is modelled using the standard k-epsilon model (14) and (15). The PDF is obtained by presuming a β-function (9). The chemical kinetics are modelled using the GRI-mechanism with 325 chemical reactions and 53 species.

The computational domain consists of 2D axisymmetric with 1000 mm in the axial direction and 153 mm in the radial direction as shown in Figure 2. The polygonal mesh type was selected to construct the physical grid with 37143 cells. The cells size is refined near to the fuel port to capture the finite-rate chemistry effects as shown in Figure 3. The smallest cell before the refinement has a size of approximately 0.5 mm.

Figure 3: Computational domain grid point.

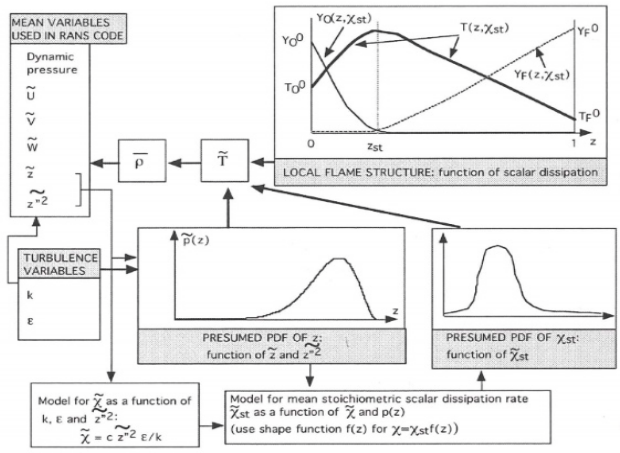

Figure 4: Presumed PDF flamelet computational steps [9].

In the flamelet method in Figure 4, a library is constructed by solving the instantaneous $Y_\alpha(z, \chi_{st})$ and $T(z, \chi_{st})$ as a function of mixture fraction and the stoichiometric dissipation rate. 100 grid points are specified for the mixture fraction and 14 different values of χ_{st} are specified to account for the stretch effects and quenching at the stoichiometry. The nonlinear differential steady governing equations for the complex flow fields are discretised using a mixed finite element method, which employs stabilisation techniques to address issues with the pressure-velocity coupling and the nonlinear convection terms. The mean quantities are obtained from the integral equation (8). 2200 iterations are specified to ensure the solution is converged as shown in Figure 5 along with the residuals.

5. Results and Discussion

The computed mean quantities are compared to the experimental measurements [17, 18] at three axial locations x/D =0.26, 0.60, 0.90, and 1.30, in the flame B4F3A, and will be discussed in this section.

The recirculation zone and the shear flow created by the bluff-body are well captured in the simulation as shown in Figure 6.

The mean passive scalar, the mixture fraction, $\tilde{z}$, and its variance, $\widetilde{z''^2}$, are solved to obtain the PDF. Figure 7 shows the computed radial variation of $\tilde{z}$ at different axial locations in the flame. Also, the contours are shown for the visual inspection. The computed values are in excellent agreement

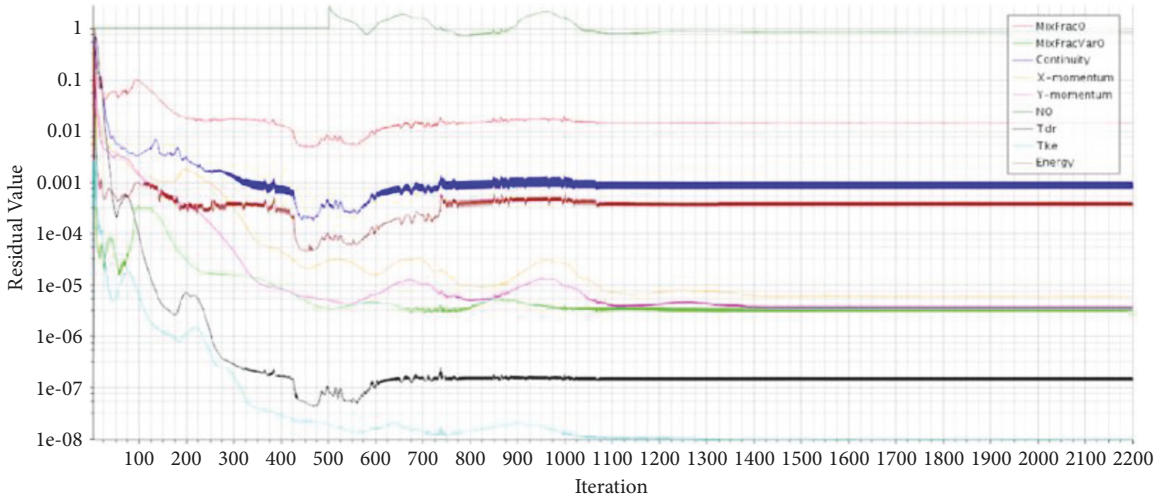

Figure 5: Residual plot.

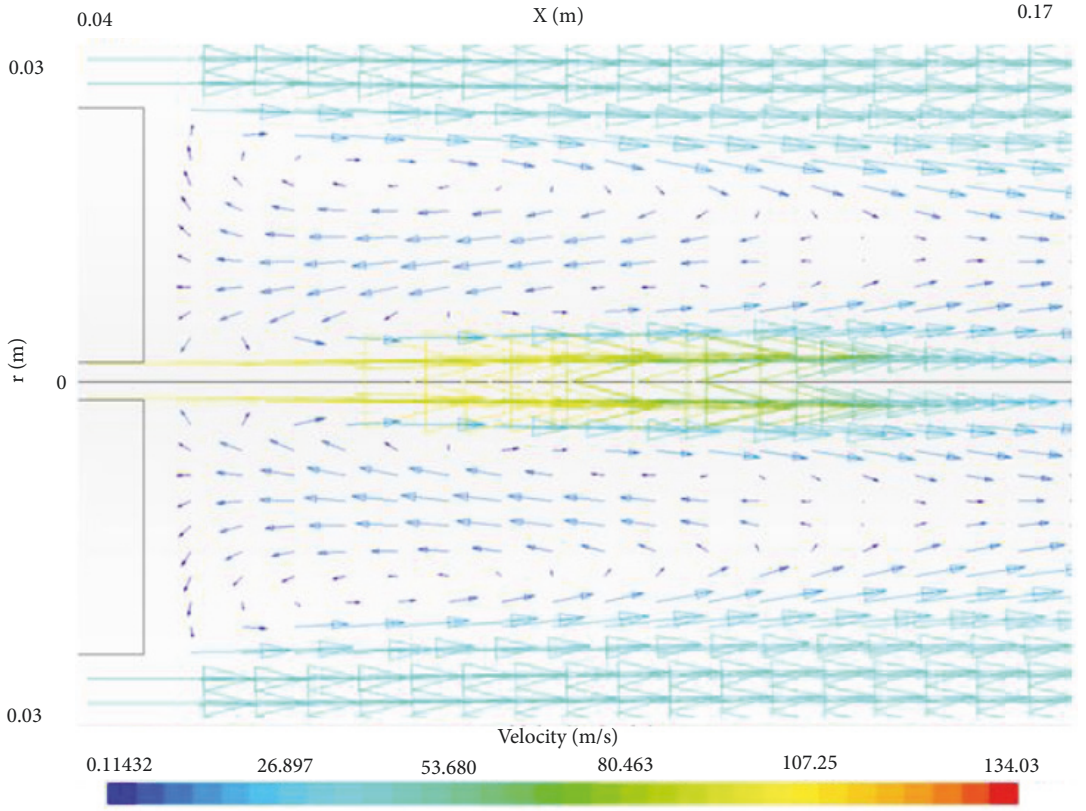

Figure 6: The recirculation zone of the flame B4F3A.

with the measurements at all three axial locations. It should be noted that the mean quantities are linked to the instantaneous values through the PDF and hence this accuracy will improve the prediction of the mean values.

The radial variations of the mean temperature are compared to the experimental measurements and are shown in Figure 8. The contours show that the flame is well developed with a maximum temperature of 2019K. This temperature is typical for this type of reactants. Despite some minor discrepancies, the computed values using the flamelet method are in good agreement with the experimental data at all axial locations. Identical levels of agreement are also observed for the major species mass fraction such as Y_{CH_4}, Y_{CO_2}, and Y_{H_2O} which are not reported in this study.

The computed mean values of the minor species CO and NO are compared to the experimental data and are shown in Figures 9 and 10. The flamelet method has captured the typical radial profile of these species. The comparison

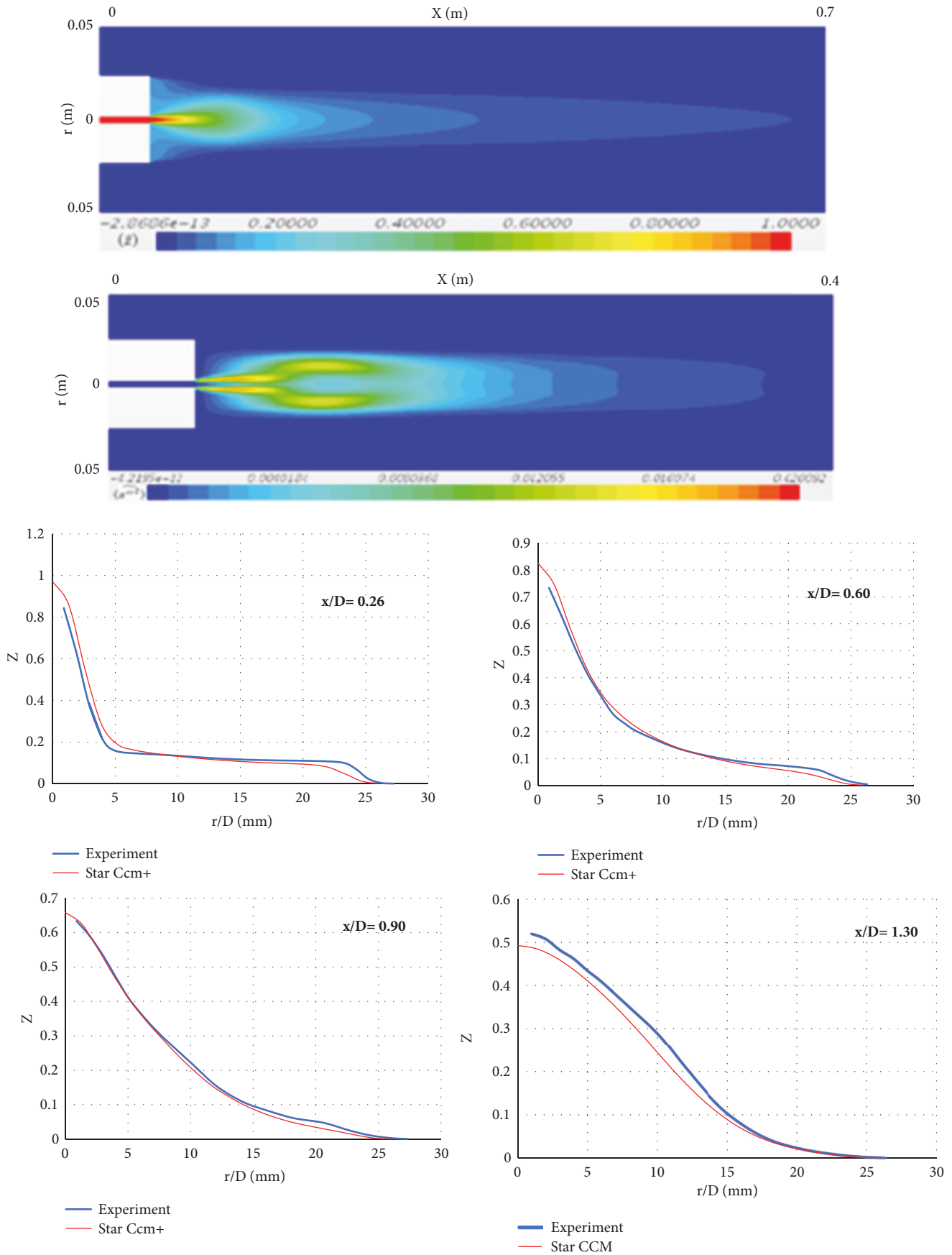

Figure 7: Contours of the mean mixture fraction for flame B4F3A and comparison to the experimental results at three axial locations.

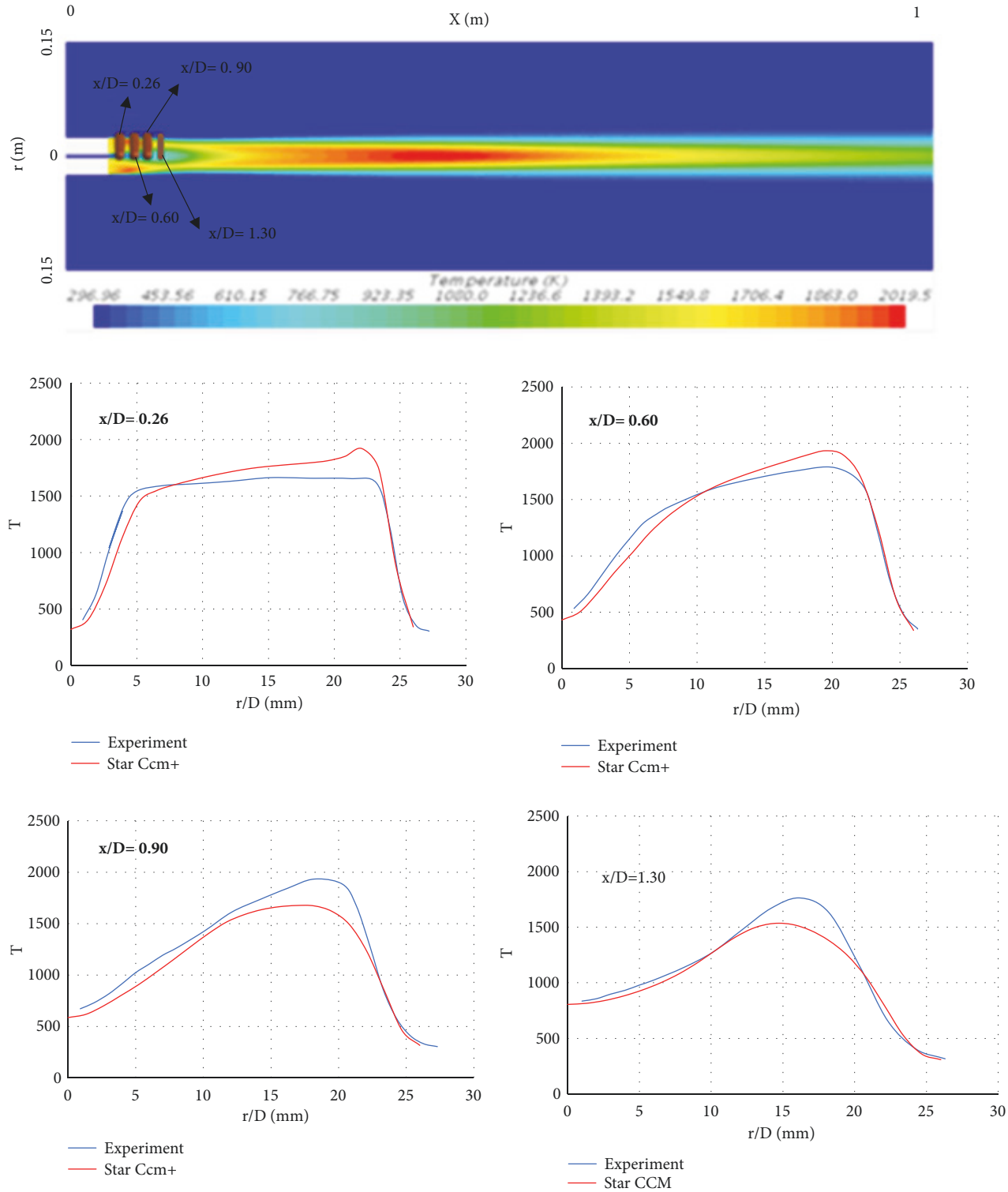

Figure 8: Contour of the mean temperature for flame B4F3A and comparison to the experimental results at three axial locations.

of CO is in good agreement upstream near the fuel port. As for the axial locations x/D = 0.60 and x/D = 0.90, some discrepancies are explicitly noticed, at radial locations $r/D > 12$. This behaviour can be attributed to the effect of turbulence and require further investigations. The agreement with experimental measurements is highly overpredicted at axial locations greater than 1.3.

The mass fractions of NO are underpredicted at all axial locations in the flame. Predicting pollutants with slow time scale such as NO from combustion systems is a challenge

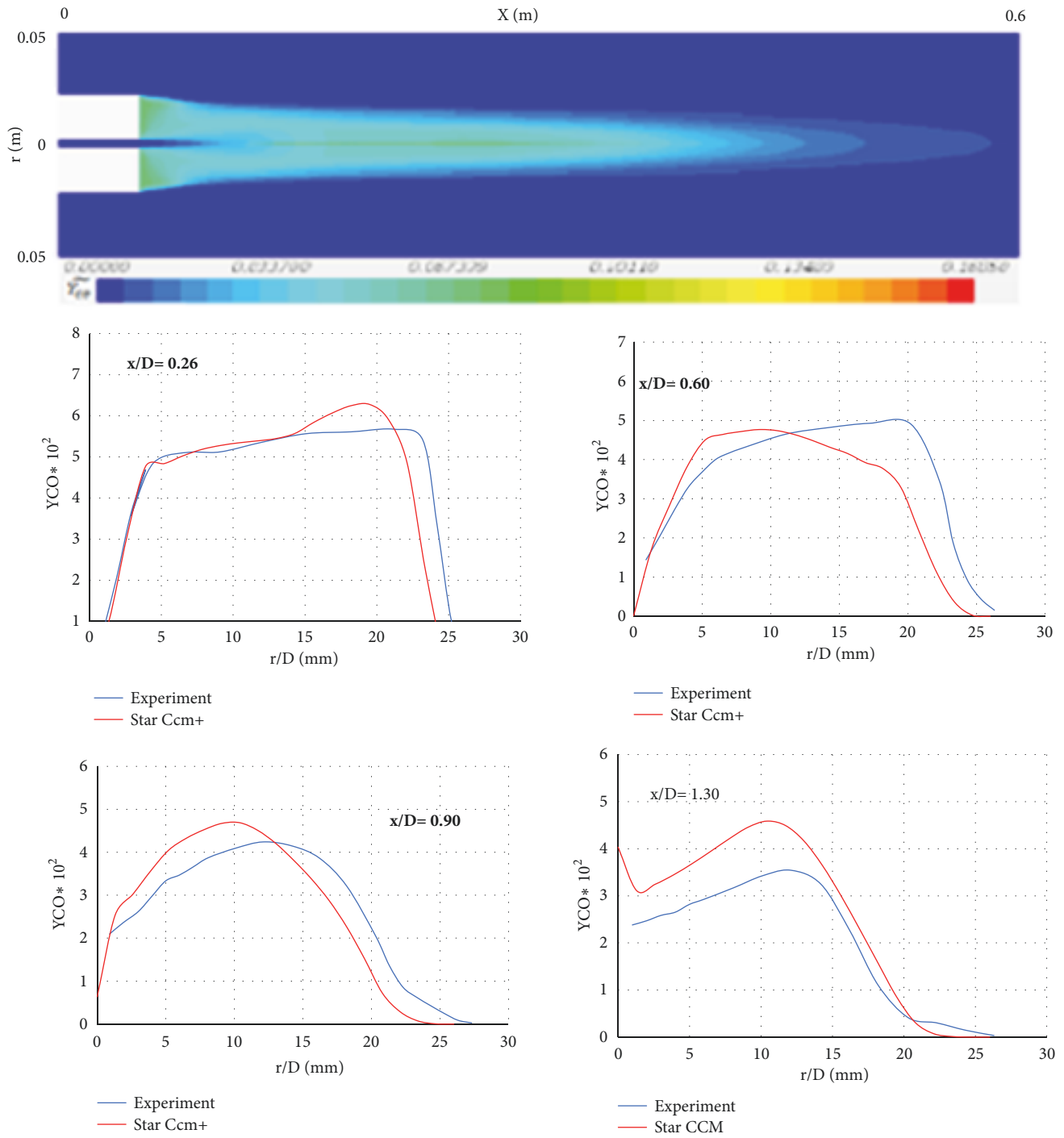

Figure 9: Contour of the mean carbon monoxide mass fraction for flame B4F3A and comparison to the experimental results at three axial locations.

for turbulent combustion modelling. These results are consistent with earlier reported studies using more complex combustion models. The reason for these discrepancies is that the flamelet model is not adequate to capture the finite-rate chemistry effects and shear turbulence specifically, for species with a slow time scale such as nitrogen oxides. Similar behaviour is noted at axial location greater than x/D = 1.3.

6. Summary and Conclusions

The overall aim of this study is to predict pollutants using the flamelet method from nonpremixed flames stabilised by a bluff-body and to compare the results with the experimental measurements, precisely, to predict pollutants with slow time scale such as CO and NO. The flamelet method is a well-established method, and it has been used in previous studies

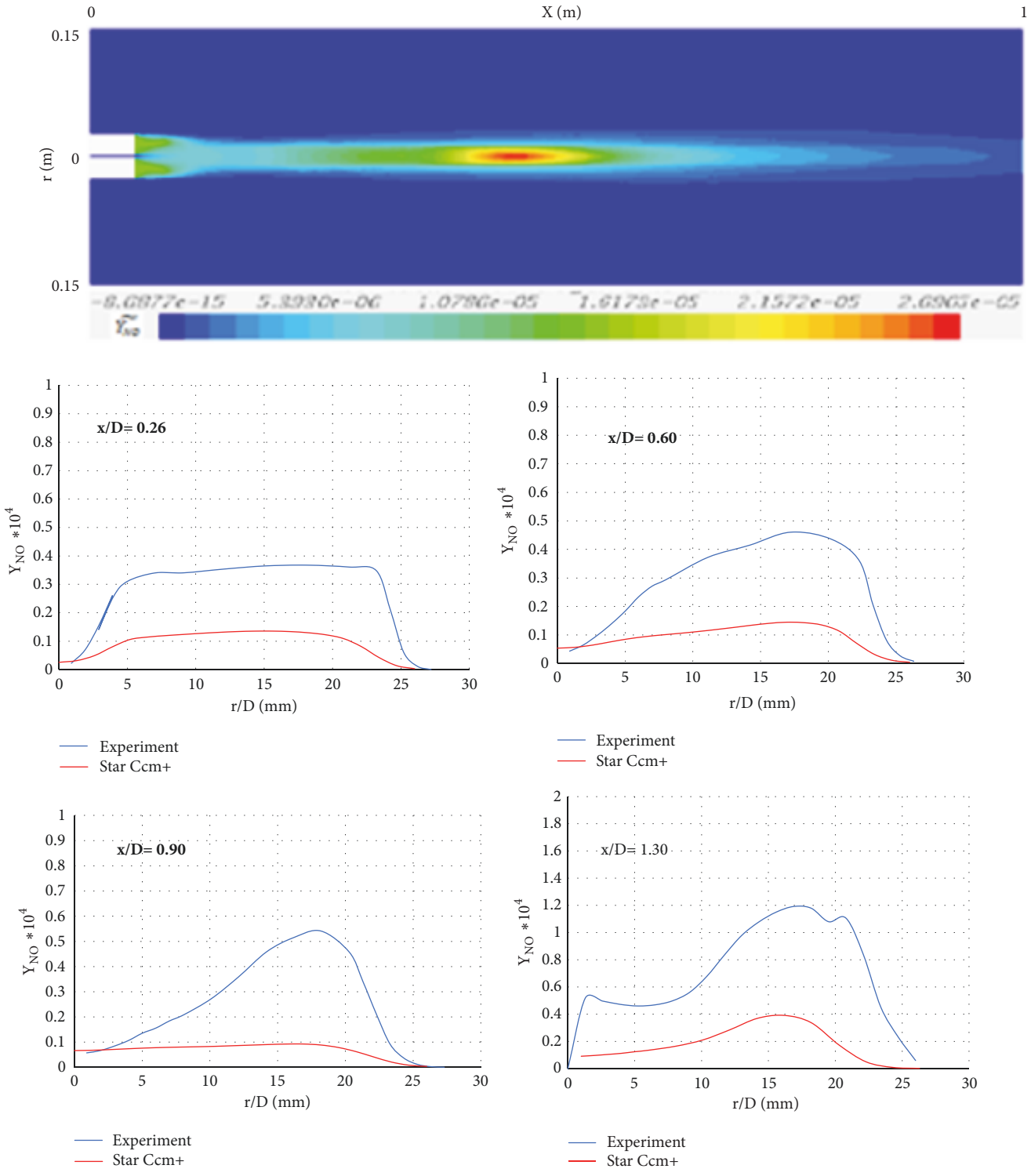

Figure 10: Contour of the mean nitrogen oxide mass fraction for flame B4F3A and comparison to the experimental results at three axial locations.

to compute nonpremixed and premixed flames in RANS and LES paradigms. The B4F3A flame, which has the lowest jet velocity, is considered to test RANS-Flamelet method. The main jet contains a (50/50% by volume) mixture of methane and hydrogen with an initial temperature of 293K. The turbulence is modelled using the standard k-ϵ model. The chemical kinetics are modelled using the GRI-mechanism, which includes the formation of CO and NO. This mechanism consists of 325 chemical reactions and 53 species. The PDF is obtained by presuming a β-function. The computed

values are observed to be in reasonably good agreement with the experimental data. Although some underpredictions are observed mainly for NO and CO at downstream locations in the flame, these results are consistent with earlier reported studies using more complex combustion models. The reason for these discrepancies is that the flamelet model is not adequate to capture the finite-rate chemistry effects and shear turbulence specifically, for species with a slow time scale such as nitrogen oxides.

Data Availability

Most of the data used to support the findings of this study are available from the corresponding author upon request. However, some computational data are not available due to size limitations.

Conflicts of Interest

The authors declare that there are no conflicts of interest regarding the publication of this paper.

References

[1] M. Maslin, *Global Warming: Causes, Effects and the Future*, LLC and Voyageur Press, Minneapolis, Minn, USA, 2007.

[2] C. N. Lane, *Acid rain: Overview and Abstracts*, Nova Science, New York, NY, USA, 2003.

[3] R. A. Houghton, "The contemporary carbon cycle," in *Treatise on Geochemistry*, D. H. Holland and K. K. Turekian, Eds., pp. 473–513, Pergamon, Oxford, UK, 2003.

[4] European Commission Statistics, *Renewable Energy Statistics*, European Commission Statistics, 2010.

[5] D. D. Rankin, *Lean Combustion Technology and Control*, Elsevier, California, Calif, USA, 1st edition, 2008.

[6] J. C. Lieuwen T. Zinn B.T., "A mechanism of combustion instability in lean premixed gas turbine combustors," *Journal of Engineering for Gas Turbines and Power*, vol. 123, no. 1, pp. 182–189, 2001.

[7] A. Masri, R. Dibble, and R. Barlow, "The structure of turbulent nonpremixed flames revealed by Raman-Rayleigh-LIF measurements," *Progress in Energy and Combustion Science*, vol. 22, no. 4, pp. 307–362, 1996.

[8] A. R. Masri, B. B. Dally, R. S. Barlow, and C. D. Carter, "The structure of the recirculation zone of a bluff-body combustor," *Symposium (International) on Combustion*, vol. 25, no. 1, pp. 1301–1308, 1994.

[9] T. Poinsot and D. Veyante, *Theoretical and Numerical Combustion*, Westview Press, Philadelphia, Pa, USA, 2005.

[10] F. A. Williams, "Turbulent combustion," in *The Mathematics of Combust*, J. D. B. Master, Ed., pp. 97–132, Society for Industrial and Applied Mathematics (SIAM), Philadelphia, Pa, USA, 1985.

[11] N. Peters, "Laminar flamelet concepts in turbulent combustion," *Symposium (International) on Combustion*, vol. 21, no. 1, pp. 1231–1250, 1988.

[12] A. Mura, F. Galzin, and R. Borghi, "A unified PDF-flamelet model for turbulent premixed combustion," *Combustion Science and Technology*, vol. 175, no. 9, pp. 1573–1609, 2003.

[13] H. Kolla and N. Swaminathan, "Strained flamelets for turbulent premixed flames, I: Formulation and planar flame results," *Combustion and Flame*, vol. 157, no. 5, pp. 943–954, 2010.

[14] H. Kolla and N. Swaminathan, "Strained flamelets for turbulent premixed flames II: Laboratory flame results," *Combustion and Flame*, vol. 157, no. 7, pp. 1274–1289, 2010.

[15] N. Peters, "Laminar diffusion flamelet models in non-premixed turbulent combustion," *Progress in Energy and Combustion Science*, vol. 10, no. 3, pp. 319–339, 1984.

[16] H. Pitsch and N. Peters, "A consistent flamelet formulation for non-premixed combustion considering differential diffusion effects," *Combustion and Flame*, vol. 114, no. 1-2, pp. 26–40, 1998.

[17] B. B. Dally, A. R. Masri, R. S. Barlow, and G. J. Fiechtner, "Turbulent non-premixed flames stabilised on a bluff-body burner," Sandia Report, 1996.

[18] "Bluff-body Flows and Falmes," http://web.aeromech.usyd.edu.au/thermofluids/bluff.php.

[19] N. Peters, *Turbulent Combustion*, Cambridge Monographs on Mechanics, Cambridge University Press, Cambridge, UK, 2000.

[20] R. Borghi, "Turbulent combustion modelling," *Progress in Energy and Combustion Science*, vol. 14, no. 4, pp. 245–292, 1988.

[21] J. Janicka and N. Peters, "Prediction of turbulent jet diffusion flame lift-off using a pdf transport equation," *Symposium (International) on Combustion*, vol. 19, no. 1, pp. 367–374, 1982.

[22] N. Swaminathan and K. N. C. Bray, *Turbulent Premixed Flames*, Cambridge University Press, Cambridge, UK, 2011.

[23] O. R. Darbyshire, *Modelling of turbulent stratified flames [Ph.D. thesis]*, The University of Cambridge, Cambridge, UK, 2011.

[24] A. R. Masri, R. W. Dibble, and R. S. Barlow, "Raman-rayleigh measurements in bluff-body stabilised flames of hydrocarbon fuels," *Symposium (International) on Combustion*, vol. 24, no. 1, pp. 317–324, 1992.

[25] A. Masri and R. Bilger, "Turbulent diffusion flames of hydrocarbon fuels stabilized on a bluff body," *Symposium (International) on Combustion*, vol. 20, no. 1, pp. 319–326, 1985.

[26] S. H. Kim and K. Y. Huh, "Use of the conditional moment closure model to predict NO formation in a turbulent CH_4/H_2 flame over a bluff-body," *Combustion and Flame*, vol. 130, no. 1-2, pp. 94–111, 2002.

[27] K. Xiao, D. Schmidt, and U. Maas, "PDF simulation of turbulent non-premixed CH4/H2-air flames using automatically reduced chemical kinetics," *Symposium (International) on Combustion*, vol. 27, no. 1, pp. 1073–1080, 1998.

[28] M. Hossain, J. C. Jones, and W. Malalasekera, "Modelling of a bluff-body nonpremixed flame using a coupled radiation/flamelet combustion model," *Flow, Turbulence and Combustion*, vol. 67, no. 3, pp. 217–234, 2002.